Structure
Ways & Means

Optically Resolving Individual Microtubules in Live Axons

Harsha V. Mudrakola,[1,2] Kai Zhang,[1,2] and Bianxiao Cui[1,*]
[1]Department of Chemistry, Stanford University, Stanford, CA 94305, USA
[2]These authors contributed equally to this work.
*Correspondence: bcui@stanford.edu
DOI 10.1016/j.str.2009.09.008

SUMMARY

Microtubules are essential cytoskeletal tracks for cargo transportation in axons and also serve as the primary structural scaffold of neurons. Structural assembly, stability, and dynamics of axonal microtubules are of great interest for understanding neuronal functions and pathologies. However, microtubules are so densely packed in axons that their separations are well below the diffraction limit of light, which precludes using optical microscopy for live-cell studies. Here, we present a single-molecule imaging method capable of resolving individual microtubules in live axons. In our method, unlabeled microtubules are revealed by following individual axonal cargos that travel along them. We resolved more than six microtubules in a 1 μm diameter axon by real-time tracking of endosomes containing quantum dots. Our live-cell study also provided direct evidence that endosomes switch between microtubules while traveling along axons, which has been proposed to be the primary means for axonal cargos to effectively navigate through the crowded axoplasmic environment.

INTRODUCTION

Neurons are morphologically polarized cells with their axons extending to lengths several orders of magnitude greater than the size of their cell bodies (Craig and Banker, 1994; Witte and Bradke, 2008). Due to the immense length of axons (up to a meter), neurons rely on active transport of vesicular cargos between the cell bodies and axon termini for proper distribution of proteins, lipids and other materials. Indeed, virtually all axonal cargos are carried to their destination by molecular motors traveling along microtubules. Kinesin motors transport cargos toward axonal termini, while dynein motors move cargos toward the cell body (Holzbaur, 2004; Vale, 2003; Vale et al., 1992). Because microtubules are the cytoskeletal tracks for axonal transportation and also the primary structural scaffold of axons (Holzbaur, 2004; Vale, 2003), assembly of microtubules is tightly regulated in axons. Disorganized microtubules have been linked to failed axonal transport and to the formation of a retraction bulb at an injured axonal site (Baas and Qiang, 2005; Erturk et al., 2007). Emerging data suggest that abnormalities in the microtubule system result in neuronal connectivity disorders in Parkinson's disease and schizophrenia (Andrieux et al., 2006; Cappelletti et al., 2005; De Vos et al., 2008).

Much of our current knowledge about the structure of microtubule assembly in axons is based on biochemical studies and electron microscopy (EM) imaging with fixed cells or tissues (Falnikar and Baas, 2009; Heidemann et al., 1984; Hirokawa, 1982; Nixon, 1998; Takahashi et al., 2007). Axonal microtubules were first revealed by EM to be evenly spaced tubular structures that run nearly parallel to each other in the longitudinal direction of axons (Bray and Bunge, 1981; Hirano and Dembitzer, 1967). In the early 1980s, Heidemann et al. (Heidemann et al., 1981; Heidemann and McIntosh, 1980) discovered that axonal microtubules have a uniform polarity with their plus ends oriented away from the cell body and their minus ends facing the soma (Conde and Caceres, 2009; Kwan et al., 2008; Witte and Bradke, 2008). Further EM studies also revealed that microtubule-associated proteins such as Tau form cross-bridge structures that regulate the structural assembly of axonal microtubules by altering their spacing and bundling (Baas and Qiang, 2005; Conde and Caceres, 2009; Dehmelt and Halpain, 2005; Ellisman and Porter, 1980; Harada et al., 1994; Yang et al., 1999). Because microtubules are essential for cargo transport within the axon, alterations in their spatial organization would inevitably affect the axonal transport process and likely play an important role in many neurological diseases (Falnikar and Baas, 2009). Although EM studies helped elucidate the structural assembly of microtubules in fixed neurons, they cannot recapitulate how axonal microtubules organize in live neurons and, most importantly, how microtubule assembly affects axonal transport.

Optical fluorescence imaging has been widely applied in life sciences because of its noninvasive, highly specific and time-resolved nature. However, the spatial resolution of lens-based optical microscopy has a physical lower bound due to the diffraction of light (Born and Wolf, 1997), which prevents resolving structures finer than half the wavelength of probing light. There are over 15 microtubules packed into a mammalian axon (500–1000 nm diameter) separated by distances (~50 nm) smaller than the diffraction limit. As a result, conventional optical microscopy cannot resolve individual axonal microtubules. A report using fluorescence speckle microscopy (FSM) has demonstrated the ability to resolve a few microtubules in the shaft region of *Xenopus* neurons where axons are as wide as 15 μm (Chang et al., 1999; Waterman-Storer et al., 1998). However, the FSM technique is still limited by the diffraction of light and cannot resolve individual microtubules when they are tightly packed in mammalian axons.

In the past few years, several superresolution imaging techniques, such as PALM (Betzig et al., 2006; Biteen et al., 2008), fPALM (Hess et al., 2006), STORM (Rust et al., 2006), STED (Donnert et al., 2006), GSDIM (Folling et al., 2008), and SSIM (Gustafsson, 2005) have emerged to defy the diffraction limit. As summarized in recent reviews (Hell, 2009; Moerner, 2007), localization-based techniques such as PALM, fPALM, and STORM take advantage of the fact that the center of the point spread function (PSF) of a single emitter can be determined to a few nanometer, a precision significantly greater than the diffraction limit of 200–300 nm (Kural et al., 2005; Moerner, 2006 ; Yildiz et al., 2003). To ensure that PSFs of individual fluorophores do not overlap in the images, photo-switchable fluorophores are used so that only a small subset of the population is converted to the fluorescent state for each imaging cycle (Bates et al., 2005; Patterson and Lippincott-Schwartz, 2002). Superresolution is achieved by repeating the activation-imaging-localization cycles for many times and subsequently combining the series of images together to reconstruct a single high-resolution image. This strategy can resolve cellular features as small as 20 nm, but it often requires minutes to hours of data collection for a high-resolution image, which hinders its application to study fast dynamic processes.

In the present study, we use simple wide-field recording combined with the localization-based strategy to perform dynamic studies in live axons at resolutions below the diffraction limit. We take advantage of the axonal transport process to separate single fluorophores so their PSFs do not overlap. We then locate the centers of moving endosomes labeled with quantum dots (QD) with high accuracy at each time point. Time-lapse positions of a moving endosome reveal the unlabeled microtubule track along which the endosome travels. This method allowed us to resolve individual axonal microtubules with their interdistance well below the diffraction limit. In particular, we have resolved more than six microtubules packed in a 1 μm diameter axon and directly observed that endosomes switch between microtubule tracks while traveling through axons.

RESULTS

Endosomal Tracking to Achieve Superresolution

The natural process of endosomal transport in axons allows for the separation of fluorophores in time and space (Figure 1A). Unlike previous strategies that achieve superresolution by switching fluorophores on and off through repeated activation-deactivation cycles, we effectively exploit the dynamic nature of moving organelles to temporally separate the otherwise spatially overlapping images. As illustrated in Figure 1A, fluorescence images of moving endosomes are recorded frame by frame. The central positions of individual endosomes can be determined to very high accuracy by fitting their PSF intensity profiles with a two-dimensional (2D) Gaussian function. By tracking endosomal central positions over time, we can map out the microtubule tracks that the organelle travels along. Cumulative trajectories of individual organelles depict densely packed cytoskeletal structures with high accuracy (Figure 1A).

We chose QD fluorophores for their high photostability, which is essential for continuous tracking of endosomal transport for long periods of time (tens of minutes). The PSF of a single molecule emitter (Bates et al., 2005; Pierobon et al., 2009), a spherical fluorescent bead or organelle containing a large number of fluorophores (Bruno et al., 2008; Kural et al., 2005), is well approximated by a 2D Gaussian profile. However, a low copy number of fluorophores generally does not project a Gaussian emission profile. Despite providing a stronger signal, multiple quantum dots in a single endosome are not beneficial for localization purposes because endosomes generally only contain a low copy number of quantum dots. Hence a single quantum dot is desired in each endosome to ensure proper fitting of the PSF with a 2D Gaussian function.

Imaging Platform for NGF Retrograde Transport

The system of axonal transport we examined was retrograde transport of nerve growth factor (NGF) in dorsal root ganglia (DRG) neurons of *Rattus norvegicus*. NGF is a member of the neurotrophin protein family that supports neuronal survival, stimulates neurite growth, and maintains proper neuronal connections (Zweifel et al., 2005). It has been shown that externally applied NGF binds to its TrkA membrane receptor located at the axon terminus and the whole NGF-TrkA complex is subsequently endocytosed into endosomes that are retrogradely transported along the axonal microtubules back to the cell body (Grimes et al., 1997; Zweifel et al., 2005). Our previous studies indicate that there is only a single NGF molecule per endosome (Cui et al., 2007). Hence by labeling individual NGF molecules with a single QD, we can apply the single molecule subdiffraction imaging to resolve individual axonal microtubules.

Imaging of NGF retrograde transport is enabled by a previously developed imaging platform specifically designed to study axonal transport (Cui et al., 2007) (Figure 1B). A pseudo total internal reflection fluorescence (TIRF) microscope, QD labeled NGF, and a sensitive EMCCD camera were used to achieve single molecule sensitivity in live neurons. DRG neurons were cultured in a microfluidic chamber (Cui et al., 2007; Taylor et al., 2003) that separated the chemical environment of the axon termini from that of the cell bodies (Figure 1B, upper panel). NGF molecules labeled 1:1 with QDs (emission max at 605 nm) were applied only to the distal axon compartment, where QD-NGF molecules bind to TrkA receptors and were endocytosed to form endosomes. Under the conditions used in this study, we measured that the vast majority (>80%) of endosomes contain a single QD-NGF complex, as identified by QD photoblinking (Cui et al., 2007). Live imaging was carried out exclusively in the microchannels or in the cell body compartment, where only successfully internalized and transported QD-containing endosomes can be observed. A low-power green laser (532 nm, 5 mW) was used as the excitation source in order to minimize phototoxicity. Under our experimental conditions, the same imaging area can be imaged continuously for greater than 30 min without any visible damage to the cells or to the axonal transport process (see Movies S1 and S2 available online).

Endosomes were observed to move exclusively toward the cell body (retrograde direction) with a ''stop-and-go'' pattern – active movements interspersed with short pauses ranging from a few hundred milliseconds to several seconds. On rare occasions, endosomes were observed to reverse their traveling direction for very short periods of time. Given the direction of transport (+ to − end) and the average velocity (~1.3 μm/s),

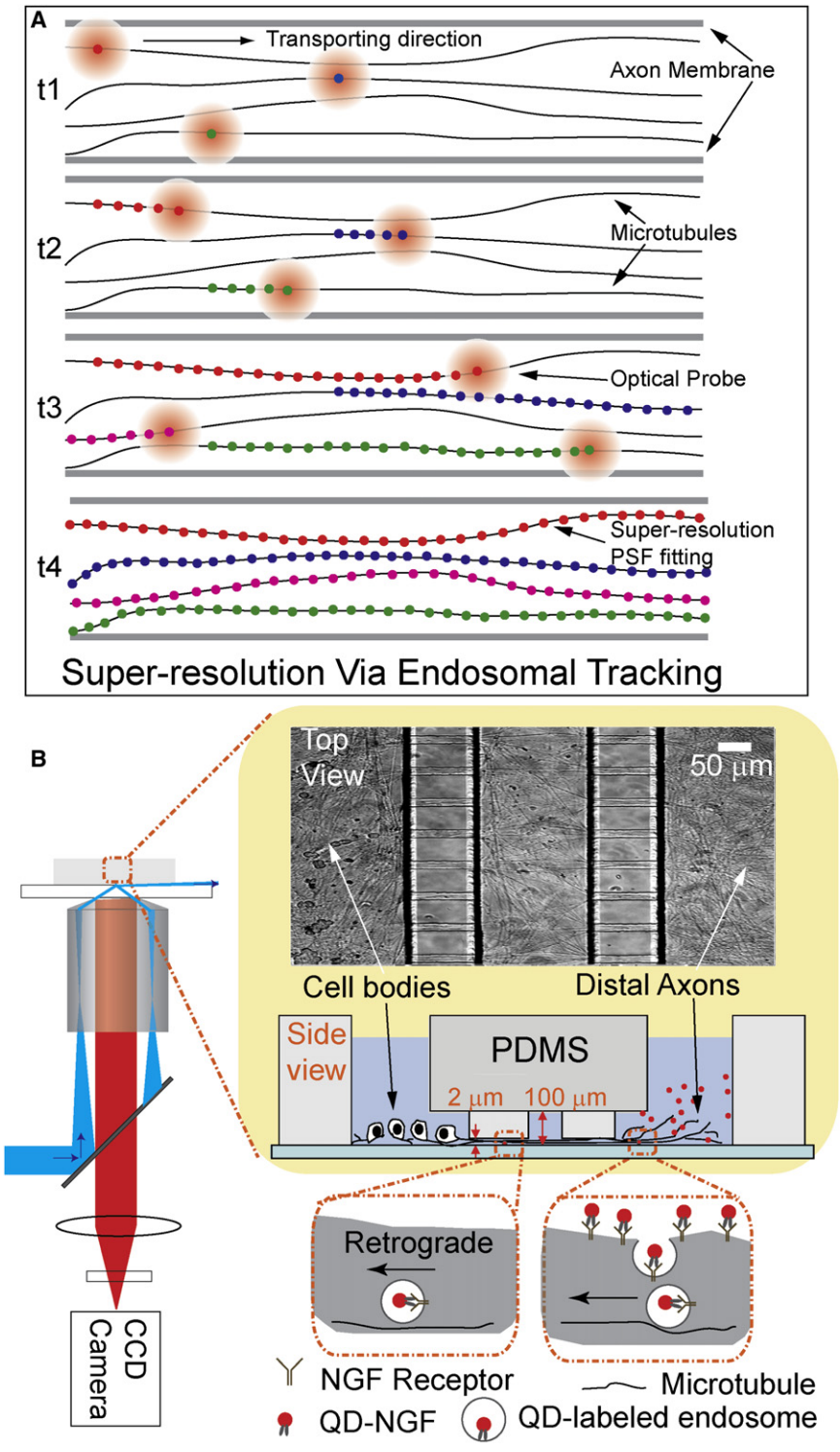

Figure 1. Schematic Representations of Imaging Strategy and Platform

(A) An illustration of imaging scheme. Fluorescently labeled organelles that are traveling along microtubules in an axon appear as large diffraction-limited spheres. At each time point, the central positions of those organelles (containing a single fluorescent molecule) are determined to high accuracy by fitting with a 2D Gaussian function. As organelles travel along the axon, their time-lapse central positions trace out the microtubule tracks that they are moving along. Cumulative trajectories depict densely packed microtubules that are otherwise unresolvable using conventional optical imaging.

(B) Platform for single molecule imaging of axonal transport. DRG neurons are cultured inside the microfluidic chamber that separates the chemical environment of the distal axons from that of the cell bodies. Fluorescent QD-NGF is applied only to the distal axons where it binds its membrane receptor and is subsequently endocytosed and retrogradely transported toward the cell body. Imaging is restricted to the microchannels or to the cell body chamber, so only internalized and transported QD-NGF molecules are observed using a pseudo-TIRF imaging setup. The angle of the incident laser beam is adjusted to be slightly less than the critical angle so the refracted beam penetrates ~1 μm into the solution.

multiple dynein motors could be involved for each endosome (Bruno et al., 2008; Kural et al., 2005; Vale, 2003). In general, we observed that endosomes proceed much longer distances (more than 40 μm) in axons compared with previous in vitro studies (Kardon et al., 2009; Mallik et al., 2005; Reck-Peterson et al., 2006), where molecular motors undergo processive movement for a characteristic length of only ~1-2 μm before they dissociate from the microtubule track. These long run lengths are likely due to microtubule-associated proteins on the endosomes and the extremely confined space in the axon, where the organelles are restricted from diffusing very far from the microtubule tracks.

Determining the Localization Accuracy

To determine the precision of our method, we first examined the localization accuracy of stationary QD-NGFs using our imaging platform. Individual QD-NGFs randomly immobilized on a glass surface were imaged for 800 successive frames at 10 frames per second. Due to the diffraction of light, each QD-NGF projected a ~4 × 4 pixel^2 PSF image (1 pixel = 0.23 μm) on the CCD camera. While the spread of the PSF imposes a lower limit on the resolving power of the optical system (>250 nm in this system), we determined the centers of the PSFs, and hence, the locations of QD-NGF to a much higher accuracy by fitting with a 2D Gaussian function (Figure 2A) (Thompson et al., 2002; Yildiz et al., 2003). A MATLAB software pipeline for large-scale processing of time-lapsed data from the imaging experiment was developed for this purpose. Figure 2B displays the spread of the determined center positions for a single QD-NGF over 321 frames. The standard deviation of

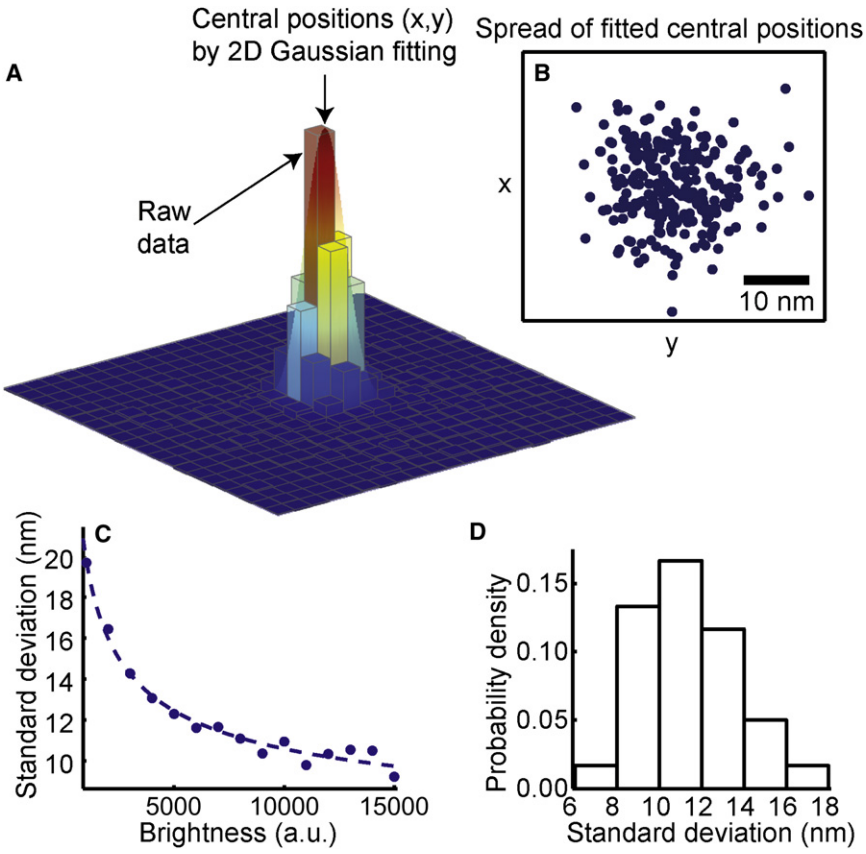

Figure 2. Localization Accuracy of Immobilized Quantum Dots

(A) The point-spread-function of a single QD-NGF molecule overlaid with the fitted 2D Gaussian function. The central position is determined to high accuracy after 2D Gaussian fitting.

(B) Spread of center positions of an immobilized quantum dot over 321 frames.

(C) Dependence of localization accuracy versus the brightness of the quantum dot. By excluding points below 5000 a.u., a centroid standard deviation of 11.5 nm was achieved.

(D) The distribution of the standard deviations of 30 QD-NGF molecules imaged over 800 frames (80 s), with the mean at 11.5 nm.

the localized center position in Figure 2B is 8.2 nm. The localization accuracy is comparable to some previously reported work of single molecules or organelle tracking in live cells (Bates et al., 2005; Pierobon et al., 2009), but lower than those reports that tracked organelles with a large number of fluorophores (Bruno et al., 2008; Kural et al., 2005). Consistent with theoretical predictions and previous observations (Thompson et al., 2002; Yildiz et al., 2003), the localization accuracy improved with increased brightness of the fluorophores (Figure 2C). Therefore, by setting a threshold for brightness and filtering out dim molecules, higher localization accuracy can be achieved. The actual resolution of the image, however, corresponds to the full-width-half-maximum (FWHM) value of the distribution of the determined center positions (Rust et al., 2006). Under our experimental conditions and averaged over 200 stationary QD-NGF molecules, standard deviation of the localized center positions was found to be 11.5 nm, which gives an actual FWHM resolution of 27 nm. Therefore, two microtubules separated by 50 nm should be resolvable.

Resolving Individual Microtubules in a Live Axon

Previous studies using EM showed axonal microtubules to be mostly rigid structures that run parallel to each other (Heidemann et al., 1984; Hirokawa, 1982). However, these analyses were performed on fixed samples and were generally limited to very short segments (usually hundreds of nanometers along the axon). Using our method, we were able to track individual moving endosomes over distances greater than 50 μm. Dynamic trajectories of individual endosomes containing a single QD-NGF were used to construct microtubule tracks that they travel along (Figure 3).

Figure 3A shows the position traces (including the dim points with lower resolutions) of 9 different endosomes over a 40-μm-long section of an axon, depicting at least 5 different microtubules. Spatial separations between different traces are fairly small because the distances between different microtubules are about 50-100 nm. We can nevertheless extract individual traces with high precision by simultaneously reconstructing the time trajectories of these observed endosomes. Figure 3B clearly shows that traces that are spatially close to each other are well separated in the time domain. For example, the magenta and blue traces spatially overlap in Figure 3A, likely due to traveling on the same microtubule; but they are well separated by > 40 s in time domain as displayed in Figure 3B. The same is true for the red and green traces.

In Figure 3C, a 5000 a.u. brightness threshold is employed to achieve 27 nm resolution traces of multiple microtubules in a single axon. Therefore, we can assign whether two traces are overlapped or separated. From this data set of 2000 frames and 14 endosomes, we traced out 6 microtubules in an axon. As seen in Figure 3, axonal microtubules are not evenly spaced over the length of the axon. Instead, they follow a similar shape determined by the curvature of the axon, parallel at times but intersecting and overlapping at other times. Zoomed-in views of three different regions provide finer structures of the microtubules (Figure 3c_1, c_2, c_3). Traces can be parallel (black and brown in Figure 3c_1), overlapped (magenta and black in Figure 3c_2), or intertwined along axons (green and gray in Figure 3c_3). Figure 3c_2 shows the magenta and black microtubules overlapping, but they are well separated in other parts of the axon as shown in Figures 3c_1 and 3c_3. Because we are observing a 2D projection of 3D structures, intersecting and short-distance overlapping are likely due to microtubules stacked on top of each other.

Capturing Dynamic Events When Endosomes Switch Microtubule Tracks

The ability to capture dynamic information at very high resolution allowed us to observe in great detail how organelles and cargos travel long distances despite the finite run length of molecular

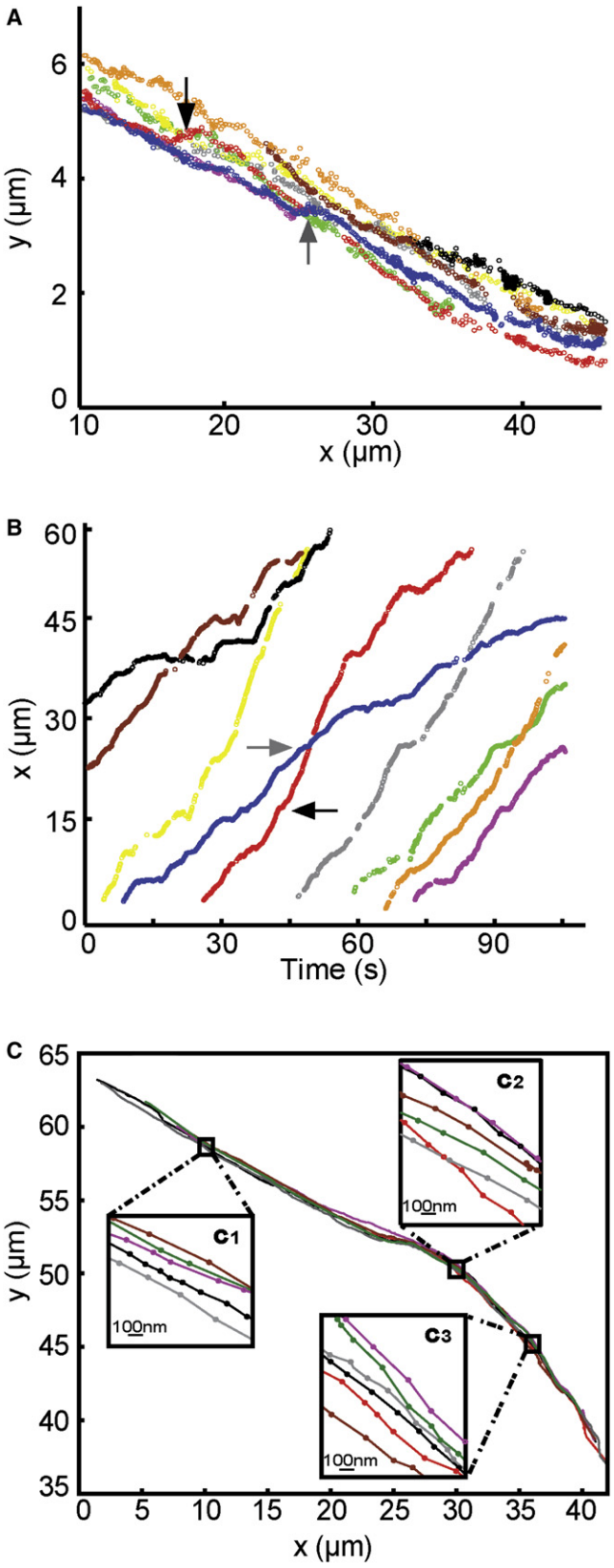

Figure 3. Resolving Individual Axonal Microtubules

A and B show the x-y positional trajectories and the corresponding x-t time traces of 9 endosomes traveling in the same axon. These trajectories include dim points that have ~70 nm FMHM resolution. Even though the trajectories are overlapped spatially, they are clearly separated in the time regime, allowing one to use the localization-based method to achieve superresolution. In (A) the red, blue, and magenta trajectories initially overlap and follow the same MT but are well separated temporally in (B). The red endosome makes a rapid lateral movement indicated by the black arrow and then proceeds along the same MT as the green endosome. Another switching event is marked for the blue trace. (C) High-resolution (~27 nm) long-distance traces constructed using a 5000 a.u. brightness cutoff. Unlike EM studies that restrict their field-of-view to several hundred nanometers, our wide-field recording method traces out microtubule structure over several tens of microns. The insets c1, c2, and c3 show zoomed-in fine structures of the microtubules. In some parts of the axon, they are overlapped (the black and purple traces in c2), but in other areas they are clearly separated.

motors and the discontinuity of the microtubule tracks. Axons contain a large number of microtubules in a highly constrained space. The question remains whether molecular motors switch between microtubule tracks while transporting endosomes inside axons. As stated earlier, dynein motor has a finite run length and will eventually dissociate from microtubules (Reck-Peterson et al., 2006; Ross et al., 2008; Schutz et al., 2004). Once dissociated, it is likely that the endosome can bind another microtubule to continue its movement. Microtubule track switching has been observed in vitro when two microtubules are directly in contact with each other (Ross et al., 2008). However, microtubule track switching in live axons has not been previously reported.

By following the dynamic trajectories of QD-NGF, we observed endosomes switching microtubule tracks during axonal transport. In Figure 3A, the red, blue, and magenta traces are initially overlapping and following the same microtubule. The red trace shows a sudden lateral movement of approximately 300 nm at the position marked by the black arrow before jumping to the same microtubule as the green trace. The gray arrow marks a similar large lateral movement for the blue trace. Corresponding black and gray arrows in Figure 3B mark the time at which these switching events occur. These lateral sharp curves of a few hundred nanometers most likely do not reflect the shape of the microtubules because the microtubule assembly is a relatively stiff chain with a large persistence length of up to 5000 μm (Pampaloni et al., 2006; van den Heuvel et al., 2007), which precludes sharp curves on the nanometer scale. We interpret these large lateral movements as events where endosomes switch microtubule tracks. This interpretation is also supported by the frequent observation of accompanying out-of-focus movements with increased Brownian motion, which is likely due to endosomes dissociated from the first microtubule before binding with a new one.

More convincing evidence came from occasions where a single endosome made a reversal of movement upon binding to a new microtubule. Figures 4A and 4B display the position and time trajectories of an endosome capturing a series of events clearly showing microtubule track switching during axonal transport (see Movie S3). The endosome initially pauses for 8 s (black) before proceeding on one microtubule in the retrograde direction (red), undergoes a y-position offset of about

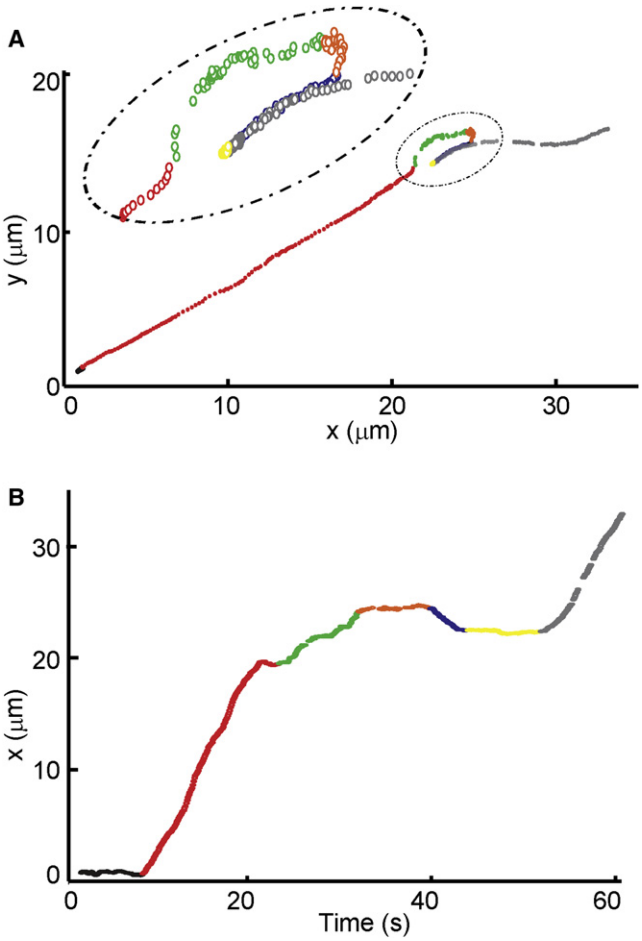

Figure 4. Capturing Microtubule Track-Switching Event During Axonal Transport

A and B display the x-y trajectory and the corresponding x-t time trace for an endosome that clearly exhibits microtubule track switching during axonal transport. The plots are colored by segments to denote a series of detailed events: initial pausing (black); directional retrograde transport (colored red); large lateral movement with continued retrograde transport (green); dissociation from the microtubule and Brownian diffusion in the cytosol (orange); association with a new microtubule and short anterograde transport (blue); a long pause (yellow) followed by retrograde transport along the new microtubule (gray) (see Movie S3).

800 nm (green), pauses and undergoes out-of-focus Brownian motion (orange), associates with a new microtubule and reverses moving direction (anterograde, blue), pauses yet another time (yellow), reverses direction again back to retrograde motion, and continues on the new microtubule (gray). Those events provided the first direct evidence that endosomes switch between different microtubules while traveling along axons in live neurons. Our ability to observe transport dynamics in great detail will enhance future studies concerning molecular mechanisms of axonal transport.

DISCUSSION

In this study, we achieved superresolution by separating molecules in both the temporal and spatial domains. Using this method, we resolved individual microtubules in live axons and directly observed endosomes switching between different microtubule tracks during axonal transport. The reconstructed microtubule traces at 27 nm resolution appear organized as shown in previous EM studies, but are not uniform over the length of the axon. They are seen to overlap and intertwine at various locations and this is reasonable given the long length of axons. Our technique makes it possible to resolve individual microtubules in a live axon and could potentially be used to characterize axonal transport and the assembly of axonal microtubules in normal and disease neurons. Furthermore, we have captured the dynamic events when endosomes switch between microtubule tracks. The ability of molecular motors to switch between microtubule tracks has been proposed to be the primary means to effectively navigate through the crowded cellular environment and deliver cargos to the appropriate location. Many neurodegenerative diseases exhibit accumulation of vesicles, organelles, or misfolded proteins insides axons, which has shown to adversely affect axonal transport (De Vos et al., 2008; Stokin et al., 2005). It is likely that endosomes will exhibit more pauses and more frequent track switching in jammed axons, and we plan to study those early events of axonal pathology.

It is worth noting the dynamic nature of the microtubule scaffold in cells. Although microtubules are very dynamic and undergo cycles of rapid growth and disassembly in growth cones, they are rather stable and have a long half-life ($t_{1/2} > 2$ hr) in mature axons where our imaging experiments were carried out (Chang et al., 1999; Conde and Caceres, 2009). Therefore, axonal microtubules appear as stable structures in our imaging time scale (2-3 min), and we frequently observe multiple endosomes traveling on the same microtubules.

Because the entire QD-NGF-TrkA complex is endocytosed into the endosome, one concern is how much of the observed movement is caused by the movement of the complex inside the endosome. Endosomes containing NGF-TrkA complexes have diameters in the range of 50-100 nm (Grimes et al., 1996; Nishida et al., 2007). Previous experiments (Yano et al., 2001) showed that TrkA receptors interact with dynein light chain, in which case the quantum dot cannot move within the endosomes. If, however, the QD-NGF-TrkA complex could freely diffuse on the endosomal membrane, we expect the QD-NGF-TrkA to sample the entire endosomal space in the 100 ms exposure time. In this case, the center of the endosome would still be accurately determined by fitting the PSF with a 2D Gaussian function. In both cases, the observed time-dependent movement will mainly come from the movement of the endosome along the microtubule.

Generally, two conditions need to be met in order to obtain superresolution images: (1) each single molecule is localized with the high accuracy; (2) the distance between individual localized points is smaller than half of the desired resolution (Nyquist criterion) (Biteen et al., 2008; Shroff et al., 2008). The Nyquist criterion ensures that the structure is adequately sampled for the desired resolution. For our method, the first condition is met as demonstrated by the 11.5 nm uncertainty for the center positions of the fluorophores. For the second condition, however, the interval distance between two adjacent points in a moving trajectory is around 130 nm (average speed 1.3 μm/s × 0.1 s time interval). This distance is larger than the desired resolution.

Nonetheless, this condition is satisfied by our knowledge that axonal microtubules are rather stiff, with persistence lengths in the millimeter range, resulting in a maximum 1.6 nm deviation from a straight line within 130 nm, which is much smaller than the localization uncertainty. Therefore, a superresolution image of microtubules can be obtained by linking adjacent localization points.

While the fluorescence image of a stationary or pausing endosome is a spherically symmetric PSF, a moving object poses a slightly elliptical fluorescence spot when integrated over time. We performed simulations to compare the accuracy of fitting both symmetric and elliptical PSFs with symmetric and asymmetric 2D Gaussian functions (Supplemental Experimental Procedures). It was found that fitting a realistic elliptical PSF with an asymmetrical Gaussian did not significantly improve localization accuracy and in some cases was worse (Table S1), likely due to numerical instability introduced by the extra fitting parameters. Considering this and to save computational time, a symmetric 2D Gaussian was chosen to analyze the neuronal movies.

Because axons are actually 3D objects, it is of enormous interest to understand how microtubules intertwine along each other and how endosomes maneuver along tangled places. This would require better resolution in all three directions. The technique presented in the current study obtained subdiffraction resolution only in 2 dimensions. The z-direction is still limited by the z-plane optical thickness (~600 nm). Recent technical developments such as controlled astigmatism (Huang et al., 2008; Kao and Verkman, 1994) and multiplane detection (Juette et al., 2008; Ram et al., 2008; Toprak et al., 2007) have achieved 40-50 nm z-resolution. Incorporation of these new techniques is currently under way, with the goal of better understanding the 3D organization of axonal microtubules in live cells and how that organization affects endosomal transport.

EXPERIMENTAL PROCEDURES

Cell Culture

DRG neurons were harvested from rat embryos of age E15 according to a published protocol (Chan et al., 2000). DRG neurons were cultured in a microfluidic chamber specially designed for neuronal culture, in which the cell bodies are grown in one chamber and the axons are directed to grow toward an adjacent chamber through microchannels (Figure 1B). Because the microchannels are only 10 μm wide and 2 μm high, the contents of the two chambers can be segregated with minimal diffusion through the microchannels. In addition, a positive pressure was created from the cell body compartment to the distal axon compartment by simply maintaining a slightly higher liquid level in the cell body compartment. This positive pressure asserts a net liquid flow toward the distal axon compartment, which further diminishes diffusion of analytes from the distal axon compartment to the cell body compartment. We exploit this capability to segregate the chemical environment of neuron cell bodies from that of the axon termini. We applied QD-NGF only to the distal axon chamber where it binds to TrkA receptors on the membrane surface of distal axons and some are internalized and sorted into endosomes. The middle compartment shown in Figure 1B was designed to further dilute any QD-NGF diffusing from the distal axon compartment through the microchannels and to prevent any QD reaching the cell body compartment.

NGF was purified from mouse submaxillary glands, biotinylated via carboxyl group substitution (Bronfman et al., 2003), and subsequently labeled with quantum dot (605 nm emission wavelength) using a streptavidin-biotin linkage according to published protocols (Cui et al., 2007). A 1:1 QD:NGF ratio was used during conjugation and 1 nM was found to be the optimal concentration of QD-NGF in order to ensure a single QD per endosome and to avoid extended overlapping of fluorescent endosomes while still getting an adequate flow through the observation area. Sporadic QD-NGF transport in the cell body compartment can be seen 30 min after application. A steady state of NGF transport is reached 3 hours later, when the image acquisition begins.

Imaging Scheme

Imaging was performed using a pseudo total internal reflection fluorescence (pseudo-TIRF) microscope built upon an inverted microscope (Nikon Ti-U) equipped with a TIRF objective (Nikon APO 60x, 1.49NA) (Figure 1B). The incident angle of the incoming excitation laser beam was kept to be slightly less than the critical angle required for complete internal reflection (Cui et al., 2007; Tokunaga et al., 2008). While most of the light was reflected at the glass-water interface like TIRF illumination, the pseudo-TIRF also resulted in a highly refracted beam that propagates at a very small angle from the glass-water surface (Figure 1B). The highly refracted beam illuminates the sample to ~1 μm deep (approximately 5 times greater than the depth of the evanescent wave used in true TIRF systems). This pseudo-TIRF configuration offers the advantage of high signal to noise ratio of traditional TIRF, while at the same time penetrates deeper into the sample. As seen in Figure 2, the imaging is restricted to the microchannels or the cell body compartment of the microfluidic culture chamber. This ensures that all QD-NGF molecules observed had been internalized at the axonal termini and transported toward the cell bodies, and circumvents the signal contamination arising from the bulk QD-NGF present in solution or non-specific binding of QD-NGF in the distal axon chamber. In order to minimize phototoxicity, QD-605 was excited with a 5 mW green laser (Spectra-Physics, 532nm), with which we can image continuously for up to 30 min at the same observation field without any visible damage to the cells.

Fluorescence signal from the quantum dot was collected by the 60 × objective, passed through a 605/20nm emission filter and detected using a back illuminated EMCCD camera (Andor iXon DU-897E, 512 × 512) with a pixel size 16 μm (corresponding to 0.23 μm at the object plane). The camera was operated at −80°C and the EM gain was set at 300, which greatly reduced contributions of readout noise. For the data shown here, movies were taken with 100 ms integration time. On average, endosomes move at 1.3 μm/s, so it takes approximately 40 s for a single endosome to cross the ~50 μm in the observation area. In order to illustrate a number of microtubules in an axon section, movies consisting of 2000-4000 fluorescence images were recorded at 0.1 s intervals.

Data Analysis

All data analysis was performed with custom-written software in MATLAB. For each frame, an 11 × 11 pixel image surrounding each individual fluorescent spot was fitted with a 2D Gaussian function by using the MATLAB nonlinear least-squares regression method.

$$P = B + A\exp\left[-\frac{1}{2}\left[\frac{(x-x_0)^2+(y-y_0)^2}{\sigma^2}\right]\right]$$

B is a constant term due to background fluorescence and detector noise. A is the amplitude that is related to the brightness of the molecule. x_0 and y_0 are the coordinates of the center, and σ is the standard deviation of the distribution held to be equal in both directions, thereby imposing a symmetric Gaussian on the PSFs. The fitted parameters are recorded for every QD-NGF PSF in every frame of a movie, allowing us to reconstruct the traces of the path taken by each molecule with high accuracy.

SUPPLEMENTAL DATA

Supplemental Data include three movies, one table, and Supplemental Experimental Procedures and can be found with this article online at http://www.cell.com/structure/supplemental/S0969-2126(09)00376-1.

ACKNOWLEDGMENTS

We thank Drs. Chengbiao Wu, Wei Wang, and Janice S. Valletta for their assistance in carrying out the experiments and helpful discussions. B.C. wishes to

express her gratitude to Prof. William W. Mobley and Prof. Yanmin Yang for their generosity in sharing resources and knowledge that significantly accelerated the research. This work was supported by National Institutes of Health grant NS057906, Bio-X interdisciplinary initiatives program, Dreyfus new faculty award, and Searle Scholar Award (to B.C.).

Received: June 19, 2009
Revised: August 21, 2009
Accepted: September 1, 2009
Published: November 10, 2009

REFERENCES

Andrieux, A., Salin, P., Schweitzer, A., Begou, M., Pachoud, B., Brun, P., Gory-Faure, S., Kujala, P., Suaud-Chagny, M.F., Hofle, G., and Job, D. (2006). Microtubule stabilizer ameliorates synaptic function and behavior in a mouse model for schizophrenia. Biol. Psychiatry *60*, 1224–1230.

Baas, P.W., and Qiang, L. (2005). Neuronal microtubules: when the MAP is the roadblock. Trends Cell Biol. *15*, 183–187.

Bates, M., Blosser, T.R., and Zhuang, X.W. (2005). Short-range spectroscopic ruler based on a single-molecule optical switch. Phys. Rev. Lett. *94*, 108101.

Betzig, E., Patterson, G.H., Sougrat, R., Lindwasser, O.W., Olenych, S., Bonifacino, J.S., Davidson, M.W., Lippincott-Schwartz, J., and Hess, H.F. (2006). Imaging intracellular fluorescent proteins at nanometer resolution. Science *313*, 1642–1645.

Biteen, J.S., Thompson, M.A., Tselentis, N.K., Bowman, G.R., Shapiro, L., and Moerner, W.E. (2008). Super-resolution imaging in live Caulobacter crescentus cells using photoswitchable EYFP. Nat. Methods *5*, 947–949.

Born, M., and Wolf, E. (1997). Principles of Optics: Electromagnetic Theory of Propagation, Interference and Diffraction of Light, 6th (corr.) Ed (Cambridge, UK; New York: Cambridge University Press).

Bray, D., and Bunge, M.B. (1981). Serial analysis of microtubules in cultured rat sensory axons. J. Neurocytol. *10*, 589–605.

Bronfman, F.C., Tcherpakov, M., Jovin, T.M., and Fainzilber, M. (2003). Ligand-induced internalization of the p75 neurotrophin receptor: a slow route to the signaling endosome. J. Neurosci. *23*, 3209–3220.

Bruno, L., Echarte, M.M., and Levi, V. (2008). Exchange of microtubule molecular motors during melanosome transport in Xenopus laevis melanophores is triggered by collisions with intracellular obstacles. Cell Biochem. Biophys. *52*, 191–201.

Cappelletti, G., Surrey, T., and Maci, R. (2005). The parkinsonism producing neurotoxin MPP+ affects microtubule dynamics by acting as a destabilising factor. FEBS Lett. *579*, 4781–4786.

Chan, J.R., Rodriguez-Waitkus, P.M., Ng, B.K., Liang, P., and Glaser, M. (2000). Progesterone synthesized by Schwann cells during myelin formation regulates neuronal gene expression. Mol. Biol. Cell *11*, 2283–2295.

Chang, S., Svitkina, T.M., Borisy, G.G., and Popov, S.V. (1999). Speckle microscopic evaluation of microtubule transport in growing nerve processes. Nat. Cell Biol. *1*, 399–403.

Conde, C., and Caceres, A. (2009). Microtubule assembly, organization and dynamics in axons and dendrites. Nat. Rev. Neurosci. *10*, 319–332.

Craig, A.M., and Banker, G. (1994). Neuronal polarity. Annu. Rev. Neurosci. *17*, 267–310.

Cui, B., Wu, C., Chen, L., Ramirez, A., Bearer, E.L., Li, W.P., Mobley, W.C., and Chu, S. (2007). One at a time, live tracking of NGF axonal transport using quantum dots. Proc. Natl. Acad. Sci. USA *104*, 13666–13671.

De Vos, K.J., Grierson, A.J., Ackerley, S., and Miller, C.C. (2008). Role of axonal transport in neurodegenerative diseases. Annu. Rev. Neurosci. *31*, 151–173.

Dehmelt, L., and Halpain, S. (2005). The MAP2/Tau family of microtubule-associated proteins. Genome Biol. *6*, 204.

Donnert, G., Keller, J., Medda, R., Andrei, M.A., Rizzoli, S.O., Lurmann, R., Jahn, R., Eggeling, C., and Hell, S.W. (2006). Macromolecular-scale resolution in biological fluorescence microscopy. Proc. Natl. Acad. Sci. USA *103*, 11440–11445.

Ellisman, M.H., and Porter, K.R. (1980). Microtrabecular structure of the axoplasmic matrix: visualization of cross-linking structures and their distribution. J. Cell Biol. *87*, 464–479.

Erturk, A., Hellal, F., Enes, J., and Bradke, F. (2007). Disorganized microtubules underlie the formation of retraction bulbs and the failure of axonal regeneration. J. Neurosci. *27*, 9169–9180.

Falnikar, A., and Baas, P.W. (2009). Critical roles for microtubules in axonal development and disease. Results Probl. Cell Differ. *48*, 47–64.

Folling, J., Bossi, M., Bock, H., Medda, R., Wurm, C.A., Hein, B., Jakobs, S., Eggeling, C., and Hell, S.W. (2008). Fluorescence nanoscopy by ground-state depletion and single-molecule return. Nat. Methods *5*, 943–945.

Grimes, M.L., Beattie, E., and Mobley, W.C. (1997). A signaling organelle containing the nerve growth factor-activated receptor tyrosine kinase, TrkA. Proc. Natl. Acad. Sci. USA *94*, 9909–9914.

Grimes, M.L., Zhou, J., Beattie, E.C., Yuen, E.C., Hall, D.E., Valletta, J.S., Topp, K.S., LaVail, J.H., Bunnett, N.W., and Mobley, W.C. (1996). Endocytosis of activated TrkA: evidence that nerve growth factor induces formation of signaling endosomes. J. Neurosci. *16*, 7950–7964.

Gustafsson, M.G.L. (2005). Nonlinear structured-illumination microscopy: Wide-field fluorescence imaging with theoretically unlimited resolution. Proc. Natl. Acad. Sci. USA *102*, 13081–13086.

Harada, A., Oguchi, K., Okabe, S., Kuno, J., Terada, S., Ohshima, T., Sato-Yoshitake, R., Takei, Y., Noda, T., and Hirokawa, N. (1994). Altered microtubule organization in small-calibre axons of mice lacking tau protein. Nature *369*, 488–491.

Heidemann, S.R., Hamborg, M.A., Thomas, S.J., Song, B., Lindley, S., and Chu, D. (1984). Spatial organization of axonal microtubules. J. Cell Biol. *99*, 1289–1295.

Heidemann, S.R., Landers, J.M., and Hamborg, M.A. (1981). Polarity orientation of axonal microtubules. J. Cell Biol. *91*, 661–665.

Heidemann, S.R., and McIntosh, J.R. (1980). Visualization of the structural polarity of microtubules. Nature *286*, 517–519.

Hell, S.W. (2009). Microscopy and its focal switch. Nat. Methods *6*, 24–32.

Hess, S.T., Girirajan, T.P., and Mason, M.D. (2006). Ultra-high resolution imaging by fluorescence photoactivation localization microscopy. Biophys. J. *91*, 4258–4272.

Hirano, A., and Dembitzer, H.M. (1967). A structural analysis of myelin sheath in central nervous system. J. Cell Biol. *34*, 555.

Hirokawa, N. (1982). Cross-linker system between neurofilaments, microtubules, and membranous organelles in frog axons revealed by the quick-freeze, deep-etching method. J. Cell Biol. *94*, 129–142.

Holzbaur, E.L.F. (2004). Motor neurons rely on motor proteins. Trends Cell Biol. *14*, 233–240.

Huang, B., Wang, W., Bates, M., and Zhuang, X. (2008). Three-dimensional super-resolution imaging by stochastic optical reconstruction microscopy. Science *319*, 810–813.

Juette, M.F., Gould, T.J., Lessard, M.D., Mlodzianoski, M.J., Nagpure, B.S., Bennett, B.T., Hess, S.T., and Bewersdorf, J. (2008). Three-dimensional sub-100 nm resolution fluorescence microscopy of thick samples. Nat. Methods *5*, 527–529.

Kao, H.P., and Verkman, A.S. (1994). Tracking of single fluorescent particles in three dimensions: use of cylindrical optics to encode particle position. Biophys. J. *67*, 1291–1300.

Kardon, J.R., Reck-Peterson, S.L., and Vale, R.D. (2009). Regulation of the processivity and intracellular localization of Saccharomyces cerevisiae dynein by dynactin. Proc. Natl. Acad. Sci. USA *106*, 5669–5674.

Kural, C., Kim, H., Syed, S., Goshima, G., Gelfand, V.I., and Selvin, P.R. (2005). Kinesin and dynein move a peroxisome in vivo: a tug-of-war or coordinated movement? Science *308*, 1469–1472.

Kwan, A.C., Dombeck, D.A., and Webb, W.W. (2008). Polarized microtubule arrays in apical dendrites and axons. Proc. Natl. Acad. Sci. USA *105*, 11370–11375.

Mallik, R., Petrov, D., Lex, S.A., King, S.J., and Gross, S.P. (2005). Building complexity: an in vitro study of cytoplasmic dynein with in vivo implications. Curr. Biol. *15*, 2075–2085.

Moerner, W.E. (2006). Single-molecule mountains yield nanoscale cell images. Nat. Methods *3*, 781–782.

Moerner, W.E. (2007). New directions in single-molecule imaging and analysis. Proc. Natl. Acad. Sci. USA *104*, 12596–12602.

Nishida, T., Arii, T., Takaoka, A., Yoshimura, R., and Endo, Y. (2007). Three-dimensional, computer-tomographic analysis of membrane proteins (TrkA, caveolin, clathrin) in PC12 cells. Acta Histochem. Cytochem. *40*, 93–99.

Nixon, R.A. (1998). Dynamic behavior and organization of cytoskeletal proteins in neurons: reconciling old and new findings. Bioessays *20*, 798–807.

Pampaloni, F., Lattanzi, G., Jonas, A., Surrey, T., Frey, E., and Florin, E.L. (2006). Thermal fluctuations of grafted microtubules provide evidence of a length-dependent persistence length. Proc. Natl. Acad. Sci. USA *103*, 10248–10253.

Patterson, G.H., and Lippincott-Schwartz, J. (2002). A photoactivatable GFP for selective photolabeling of proteins and cells. Science *297*, 1873–1877.

Pierobon, P., Achouri, S., Courty, S., Dunn, A.R., Spudich, J.A., Dahan, M., and Cappello, G. (2009). Velocity, processivity, and individual steps of single myosin V molecules in live cells. Biophys. J. *96*, 4268–4275.

Ram, S., Prabhat, P., Chao, J., Ward, E.S., and Ober, R.J. (2008). High accuracy 3D quantum dot tracking with multifocal plane microscopy for thestudy of fast intracellular dynamics in live cells. Biophys. J. *95*, 6025–6043.

Reck-Peterson, S.L., Yildiz, A., Carter, A.P., Gennerich, A., Zhang, N., and Vale, R.D. (2006). Single-molecule analysis of dynein processivity and stepping behavior. Cell *126*, 335–348.

Ross, J.L., Shuman, H., Holzbaur, E.L., and Goldman, Y.E. (2008). Kinesin and dynein-dynactin at intersecting microtubules: motor density affects dynein function. Biophys. J. *94*, 3115–3125.

Rust, M.J., Bates, M., and Zhuang, X. (2006). Sub-diffraction-limit imaging by stochastic optical reconstruction microscopy (STORM). Nat. Methods *3*, 793–795.

Schutz, G.J., Axmann, M., Freudenthaler, S., Schindler, H., Kandror, K., Roder, J.C., and Jeromin, A. (2004). Visualization of vesicle transport along and between distinct pathways in neurites of living cells. Microsc. Res. Tech. *63*, 159–167.

Shroff, H., Galbraith, C.G., Galbraith, J.A., and Betzig, E. (2008). Live-cell photoactivated localization microscopy of nanoscale adhesion dynamics. Nat. Methods *5*, 417–423.

Stokin, G.B., Lillo, C., Falzone, T.L., Brusch, R.G., Rockenstein, E., Mount, S.L., Raman, R., Davies, P., Masliah, E., Williams, D.S., and Goldstein, L.S.B. (2005). Axonopathy and transport deficits early in the pathogenesis of Alzheimer's disease. Science *307*, 1282–1288.

Takahashi, D., Yu, W., Baas, P.W., Kawai-Hirai, R., and Hayashi, K. (2007). Rearrangement of microtubule polarity orientation during conversion of dendrites to axons in cultured pyramidal neurons. Cell Motil. Cytoskeleton *64*, 347–359.

Taylor, A.M., Rhee, S.W., Tu, C.H., Cribbs, D.H., Cotman, C.W., and Jeon, N.L. (2003). Microfluidic multicompartment device for neuroscience research. Langmuir *19*, 1551–1556.

Thompson, R.E., Larson, D.R., and Webb, W.W. (2002). Precise nanometer localization analysis for individual fluorescent probes. Biophys. J. *82*, 2775–2783.

Tokunaga, M., Imamoto, N., and Sakata-Sogawa, K. (2008). Highly inclined thin illumination enables clear single-molecule imaging in cells. Nat. Methods *5*, 159–161.

Toprak, E., Balci, H., Blehm, B.H., and Selvin, P.R. (2007). Three-dimensional particle tracking via bifocal imaging. Nano Lett. *7*, 2043–2045.

Vale, R.D. (2003). The molecular motor toolbox for intracellular transport. Cell *112*, 467–480.

Vale, R.D., Malik, F., and Brown, D. (1992). Directional Instability of Microtubule Transport in the Presence of Kinesin and Dynein, 2 Opposite Polarity Motor Proteins. J. Cell Biol. *119*, 1589–1596.

van den Heuvel, M.G., Bolhuis, S., and Dekker, C. (2007). Persistence length measurements from stochastic single-microtubule trajectories. Nano Lett. *7*, 3138–3144.

Waterman-Storer, C.M., Desai, A., Bulinski, J.C., and Salmon, E.D. (1998). Fluorescent speckle microscopy, a method to visualize the dynamics of protein assemblies in living cells. Curr. Biol. *8*, 1227–1230.

Witte, H., and Bradke, F. (2008). The role of the cytoskeleton during neuronal polarization. Curr. Opin. Neurobiol. *18*, 479–487.

Yang, Y., Bauer, C., Strasser, G., Wollman, R., Julien, J.P., and Fuchs, E. (1999). Integrators of the cytoskeleton that stabilize microtubules. Cell *98*, 229–238.

Yano, H., Lee, F.S., Kong, H., Chuang, J.Z., Arevalo, J.C., Perez, P., Sung, C.H., and Chao, M.V. (2001). Association of Trk neurotrophin receptors with components of the cytoplasmic dynein motor. J. Neurosci. *21*, RC125.

Yildiz, A., Forkey, J.N., McKinney, S.A., Ha, T., Goldman, Y.E., and Selvin, P.R. (2003). Myosin V walks hand-over-hand: single fluorophore imaging with 1.5-nm localization. Science *300*, 2061–2065.

Zweifel, L.S., Kuruvilla, R., and Ginty, D.D. (2005). Functions and mechanisms of retrograde neurotrophin signalling. Nat. Rev. Neurosci. *6*, 615–625.